The integration of a scramjet as one of the stages of a multi-stage space launch system has the potential to allow for small payloads to be delivered cheaply and to orbit by a reusable system. This paper determines the maximum payload to orbit trajectory of a multi-stage rocket-scramjet-rocket system. This trajectory has been calculated by formulating the problem as an optimal control problem, then solving it using the pseudospectral method. The optimal trajectory for the scramjet stage was found to be split into two parts: a constant dynamic pressure path and a pull-up manoeuvre. This pull up manoeuvre results in a 19.1% improvement in payload mass to orbit when compared to a constant dynamic pressure trajectory with no pull-up. Furthermore, this pull-up manoeuvre decreases the maximum dynamic pressure experienced by the final rocket stage by 44.4%. The maximum dynamic pressure allowable for the scramjet was varied by $\pm$5kPa and shown to produce only a $+0.86\%$ and -2.42% variation in the payload mass to orbit. The drag produced by the vehicle was increased by 10% and was shown to produce only minimal difference in the optimal trajectory, indicating that the solution is robust to variation in trajectory and vehicle design.

Trajectory Design of a Rocket-Scramjet-Rocket Multi-Stage Launch System

Sholto O. Forbes-Spyratos* , Michael P. Kearney † , Michael K. Smart ‡ and Ingo H. Jahn §
The University of Queensland, Queensland, Australia, 4072

Nomenclature

I_{sp}	=	Specific Impulse (s)	L_N	=	Legendre Polynomial
w_k	=	Weighting Function	D	=	Differentiation Matrix
t	=	Time	τ	=	Normalised Time Scale
N	=	Node Number	t	=	Time (s)
$\mathbf{x}$	=	Primal Variables	$\mathbf{u}$	=	Control Variables
q	=	Dynamic Pressure (Pa)	f, g, ψ, λ, M, P	=	Functions
C	=	Cost Function	F	=	Force (N)
ρ	=	Density (kg/m^2)	c	=	Aerodynamic Coefficient
v	=	Velocity (m/s)	A	=	Reference Area (m^2)
H	=	Horizontal Position (m)	g_0	=	Gravitational Acceleration at Earth's Surface (m/s^2)
V	=	Vertical Position (m)	γ	=	Trajectory Angle (rad)
ω	=	Angular Velocity (rad/s)	a	=	Acceleration (m/s^2)
m	=	Mass (kg)	T	=	Thrust (N)
w_{cap}	=	Capture Width	α	=	Angle of Attack (rad)
ϕ	=	Equivalence Ratio			
Subscripts					
1	=	1^{st} Stage Rocket	2	=	2^{nd} Stage Scramjet Vehicle
3	=	3^{rd} Stage Rocket	$\rightarrow$	=	Stage Transition
d	=	Drag	L	=	Lift
s	=	Specific	f	=	Fuel
$*$	=	Payload	LOX	=	Liquid Oxygen
LH2	=	Liquid Hydrogen	b	=	End of Third Stage Burn

*Ph.D. Candidate, Centre for Hypersonics, School of Mechanical and Mining Engineering. Member AIAA.
†Lecturer, School of Mechanical and Mining Engineering.
‡Professor, Centre for Hypersonics, School of Mechanical and Mining Engineering. Senior Member AIAA.
§Lecturer, Centre for Hypersonics, School of Mechanical and Mining Engineering. Member AIAA.

I. Introduction

Currently most small satellite launches co-manifest with a larger payload, leaving their launch schedule and trajectory at the mercy of the major payload. The demand for small payload launches is increasing,[1] driving the development of cheap and efficient launch systems for independent launches of small payloads. A multi-stage launch system incorporating a scramjet second stage has been proposed as a dedicated small satellite launch vehicle.[2] Scramjets (supersonic combustion ramjets) are airbreathing engines that operate over Mach numbers in the hypersonic range.[3] Scramjet engines are a primary candidate for powering the next generation of small payload launch vehicles, producing higher specific impulse (I_{sp}) than rockets within their operating range and providing key operability benefits. These include increased flexibility of launch windows and an increased range of mission capabilities.[4] Scramjets can accelerate a launch vehicle without the need to carry oxidiser on board, providing weight savings compared to rocket-powered vehicles. The reduction of weight carried within the vehicle fuselage enables the integration of avionics and landing gear, allowing for the design of a reusable vehicle in the style of conventional aerospace vehicles. However, a launch system must contain engines capable of accelerating the scramjet to its operating speed and also placing the payload in orbit.

This paper presents a trajectory for a rocket-scramjet-rocket vehicle, designed using optimal control methods. This paper utilises a rocket-scramjet-rocket multi-stage launch system that has been proposed at the Centre for Hypersonics at The University of Queensland.[2] The trajectory profile of multi-stage vehicles has typically been designed around the scramjet stage flying a constant dynamic pressure trajectory.[5–7] A constant dynamic pressure trajectory follows the maximum dynamic pressure that the scramjet powered vehicle is able to withstand structurally, ensuring maximum thrust production from the scramjet engines. Such a trajectory produces maximum acceleration from the scramjet stage but may not be optimal for the multi-stage system. A constant dynamic pressure trajectory may be suboptimal due to the separation of the final stage into a high dynamic pressure environment, at a potentially suboptimal trajectory angle. This may result in suboptimal performance of the final stage rocket and the inclusion of unnecessary design constraints.

Launch vehicles utilising rocket and airbreathing propulsion within a single stage have previously been shown to fly at maximum dynamic pressure for the majority of airbreathing operation, followed by a pull-up before airbreathing engine cut-off.[8–10] A pull-up produces an overall favourable trade-off by allowing for the airbreathing engines to be used to increase the altitude of the launch vehicle, with the downside of reducing the thrust of the airbreathing engine due to a lower mass flow rate into the engine. The increase in altitude and trajectory angle produced by a pull-up manoeuvre results in the rocket engines being ignited at higher altitude, allowing the rocket to operate with reduced drag. A trajectory involving a pull-up has been shown to be the optimal trajectory for vehicles where the rocket engines are not ignited until circularization altitude[8,9] as well as vehicles where the rocket engine is ignited immediately after airbreathing engine cut-off.[10]

For launch systems with airbreathing and rocket propulsion combined within a single stage, the pull-up manoeuvre is a simple trade-off between velocity and altitude. However, for the proposed scramjet-rocket multi-stage system, the scramjet stage and rocket stage are sequential and are separated completely. The resultant change in mass and aerodynamic characteristics adds to the complexity of the trajectory analysis. For a robust multi-stage trajectory design there is a trade-off between the high efficiency of the scramjet engine, the thrust produced, the energy necessary to increase the altitude of the scramjet stage, and the aerodynamic efficiency when performing the required direction change. A pull-up manoeuvre has previously been identified as having potential advantages for a multi-stage airbreathing-rocket system.[11] However, these advantages were observed in a suboptimal trajectory with variation in dynamic pressure throughout multiple modes of airbreathing engine operation. The inherent complexity of a multi-stage system delivering payload to orbit necessitates an investigation into the optimal launch trajectory design.

This paper utilises optimal control theory to generate the optimal trajectory path for a rocket-scramjet-rocket multi-stage vehicle. Optimal control theory allows a trajectory to be optimised in its entirety and has been widely used in aerospace applications for computing trajectories when there is a global objective to be optimised, such as minimum fuel or maximum payload delivery.[12–14] Optimal control is also extremely flexible, as the objective of the optimal control routine can be modified easily to investigate a range of trajectory targets.[15] Complex optimal control problems (such as a highly nonlinear model of hypersonic flight) necessitate the use of direct methods such as direct single shooting, multiple shooting, or collocation. The pseudospectral collocation method of optimal control is utilised in this study due to its accuracy, efficiency, and radius of convergence when compared to other optimal control techniques.[16,17]

The remainder of the paper is as follows: Section II presents models of the three stages, including the

engine models. Section III presents an overview of the optimal control theory used including the problem definition and a description of the pseudospectral method. Section IV presents results validating the use of the pseudospectral method, optimal trajectory results for a range of maximum dynamic pressure conditions, and optimal trajectory results with variation in the vehicle's aerodynamic characteristics.

II. Problem Description

The simulated system includes a rocket powered first stage, a scramjet powered second stage, and a rocket powered third stage for payload delivery to heliosynchronous orbit. The following section details the models used for all three stages.

II.A. The First Stage Rocket

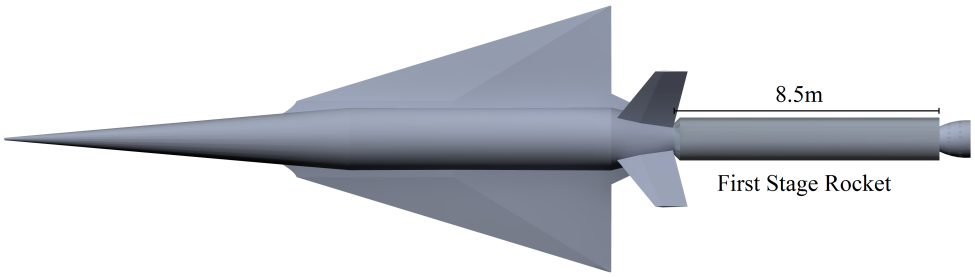

Figure 1. Model of the first stage rocket and scramjet vehicle.

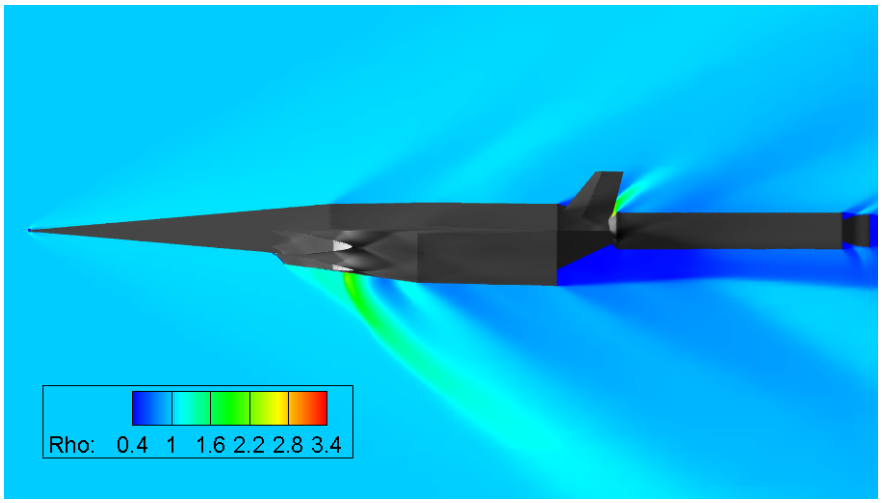

Figure 2. Normalised density contours of first stage flight, Mach 2, -1° angle of attack.

The first stage rocket, shown in Figure 1, is required to deliver to second stage to near horizontal flight at flight conditions of 50kPa dynamic pressure. To achieve this, the first stage rocket is modelled as a Falcon-1 first stage scaled down lengthwise. The first stage has a diameter of 1.67m, a length of 8.5m and a total mass of 16000kg. The first stage is attached to the rear of the scramjet second stage and is powered by a single Merlin 1-C engine. It is discarded once 50kPa dynamic pressure separation conditions are reached.

An aerodynamic database of the entire vehicle has been generated using CART3D,[18] a high-fidelity inviscid analysis CFD package with adjoint based mesh refinement. The CART3D package uses a Cartesian cut-cell approach[19] resulting in a mesh of cubes everywhere except at body-intersecting cells. CART3D has been used successfully in a variety of aerospace applications including hypersonic launch systems[20] and has

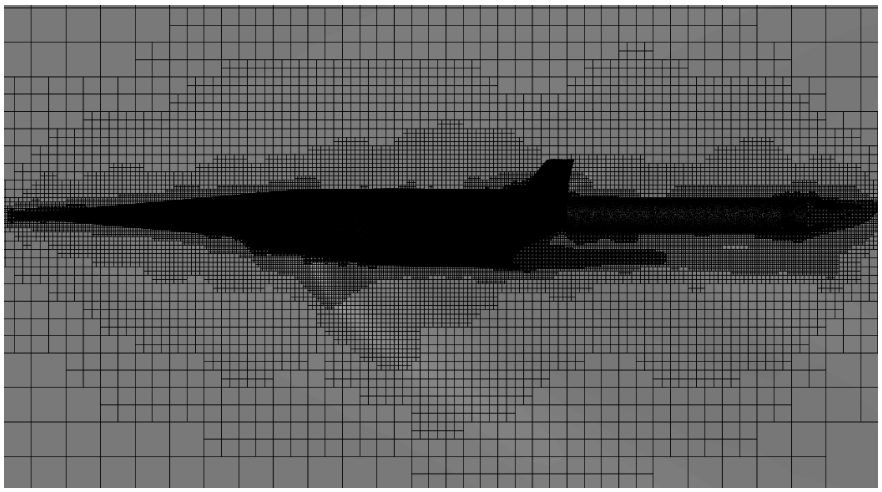

Figure 3. Adaptive mesh generated close to vehicle by CART3D for Mach 2, -1° angle of attack flight conditions.

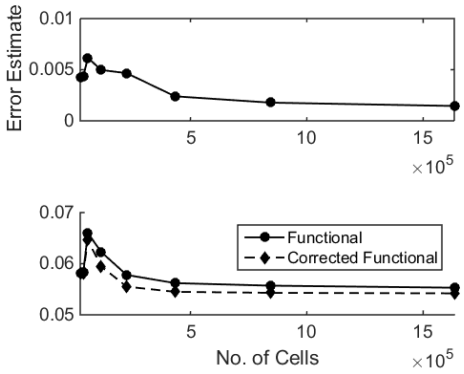

Figure 4. CART3D verification parameters.

shown good agreement when compared to experimental results.[21] For the simulation the vehicle geometry is created using Creo Parametric 3.0[22] and a body fitted triangular mesh is generated using Pointwise 18.0.[23]

A pressure field for Mach 2, -1° angle of attack is shown in Figure 2. Figure 3 shows an example of the mesh produced by CART3D. This mesh extends out to 50 body lengths at far-field boundaries. Figure 4 examines convergence parameters of the CFD solution; the functional, its adjoint-based correction and error estimate. The functional and corrected functional converge and error estimate decreases steadily as the mesh is refined, indicating mesh convergence.

II.B. The Scramjet Accelerator

The Scramjet Powered Accelerator for Reusable Technology AdvaNcement (SPARTAN) is a scramjet powered accelerator under development by the University of Queensland to be used as the second stage in a scramjet-rocket powered system for delivering small payloads to heliosynchronous orbit, carrying a rocket stage in a recess on the top of the vehicle to reduce aerodynamic drag, as shown in Figure 5.[7,24] The SPARTAN is designed to be capable of flying back after separation to a designated landing point where recovery of the vehicle is possible without damage to the system. The SPARTAN is utilised in this study as a representative model for future multi-stage access to space systems incorporating airbreathing second stages.

The SPARTAN has a fuselage diameter of 2.1m and has been sized to hold the third stage rocket and propellant tanks within the fuselage to reduce aerodynamic drag, as shown in Figure 6. Previous studies have indicated that using the SPARTAN as part of a three stage access to space system can produce payload mass fractions that compare favourably with similarly sized rocket systems.[7]

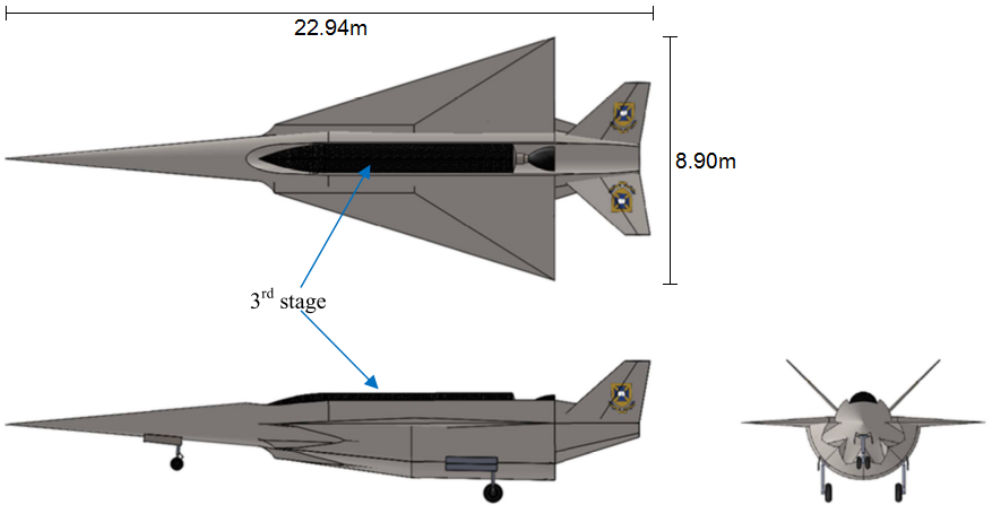

Figure 5. CAD model of the SPARTAN accelerator.[7]

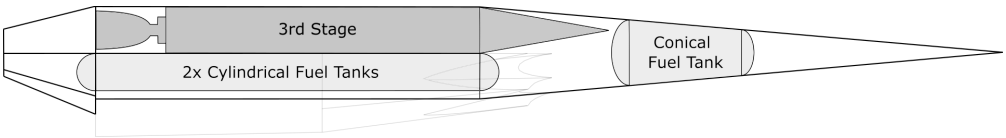

Figure 6. Internal schematic view of the SPARTAN accelerator.[7]

II.B.1. SPARTAN Aerodynamics and Engine Modelling

The aerodynamics of the SPARTAN are simulated using a set of aerodynamic coefficients developed in HYPAERO.[25] HYPAERO utilises longitudinal strip theory to provide aerodynamic coefficients over the operating range of Mach numbers, angle of attacks and flap deflection angles of the vehicle. Atmospheric properties are drawn from the U.S. Standard Atmosphere 1976.[26]

The SPARTAN is powered by four scramjet engines located on the bottom portion of the fuselage, sized to a nominal capture width of 0.65m. These engines are based on the Rectangular-to-Elliptical Shape Transition (REST) scramjet engine design[27] with modified inlets to fit to a conical fuselage via a C-REST inlet configuration.[28] The engine model used is based on the RESTM12 database, a set of experimental data for a REST engine at off-design conditions,[27] which provides data points of engine performance over inlet conditions within the operational range, at 50kPa dynamic pressure equivalent conditions. This data is interpolated for the given inlet conditions to calculate the exit conditions and the specific impulse produced by the engine. The thrust, T, is then obtained by inclusion of the mass flow rate ($\dot{m}$) obtained via the inlet conditions, ie. $T = g_0 \dot{m} I_{sp}$. The C-REST engine is a fixed geometry engine, designed for operability at high Mach numbers. At lower Mach numbers, addition of excessive fuel may cause the engine to choke and unstart. This causes the engine to reach operability limits at lower Mach numbers, necessitating an equivalence ratio (ϕ) of less than 1.

II.C. The Third Stage Rocket

At the end of the SPARTAN acceleration, the third stage rocket stage disengages and performs an altitude increasing manoeuvre to achieve orbit. The third stage rocket flight initiates with an in-atmosphere burn at positive angle of attack. At the end of the burn time the angle of attack is adjusted to 0°, and the rocket is allowed to coast until reaching horizontal flight. The end altitude is limited to a minimum of 160km to ensure that the rocket is in an exoatmospheric orbit. The orbit is circularised using a short burn, after which the final section of the payload delivery to heliosynchronous orbit is computed using a simple Hohmann transfer and orbital inclination change.

To achieve this manoeuvre, the third stage rocket (Figure 7) has a total length of 8.73m, diameter of 1.54m and a total mass of 2867kg. It is powered by a Pratt & Whitney RL-10A-4-2. The payload is located at the

Figure 7. Schematic of the third stage rocket.

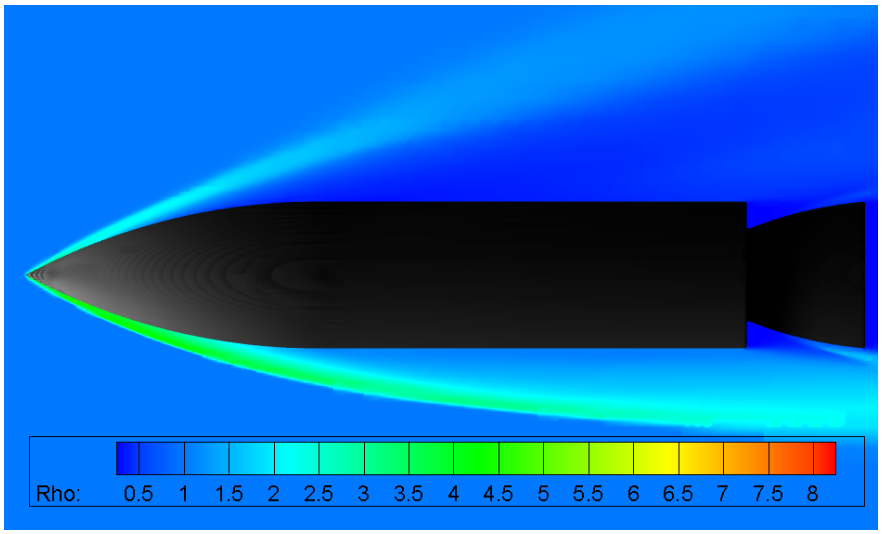

Figure 8. Third stage rocket normalised density contours for Mach 9, 10° angle of attack conditions.

nose of the rocket with a nominal size of $L_* = 0.075 L_{rocket}$ where $L_{rocket} = L_{eng} + L_{LOX} + L_{LH2} + 3L_{interface}$. The in-atmosphere separation of the rocket stage requires the use of a large heat shield that envelopes the rocket stage. The heat shield is constructed from Carbon-Carbon, weighing 302kg, and is discarded when the rocket has reached a dynamic pressure of 10Pa (atmospheric heating is assumed to be negligible at this point).[7] An aerodynamic database of the third stage rocket has been generated using CART3D. Figure 8 shows an example pressure field for Mach 9, 10° angle of attack conditions. Figure 9 shows the corresponding adaptive mesh generated by CART3D.

II.D. Dynamics Modelling

The drag and lift produced by the vehicle are calculated using the standard definition of the aerodynamic coefficients:

$$F_d = \frac{1}{2}\rho c_d v^2 A, \tag{1}$$

$$F_L = \frac{1}{2}\rho c_L v^2 A. \tag{2}$$

The dynamics of all stages are calculated using an geodetic rotational reference frame, written in terms of the radius from centre of Earth r, longitude ξ, latitude ϕ, flight path angle γ, velocity v and heading angle ζ. The equations of motion are:[29]

$$\dot{r} = v \sin\gamma \tag{3}$$

$$\dot{\xi} = \frac{v \cos\gamma \cos\zeta}{r \cos\phi} \tag{4}$$

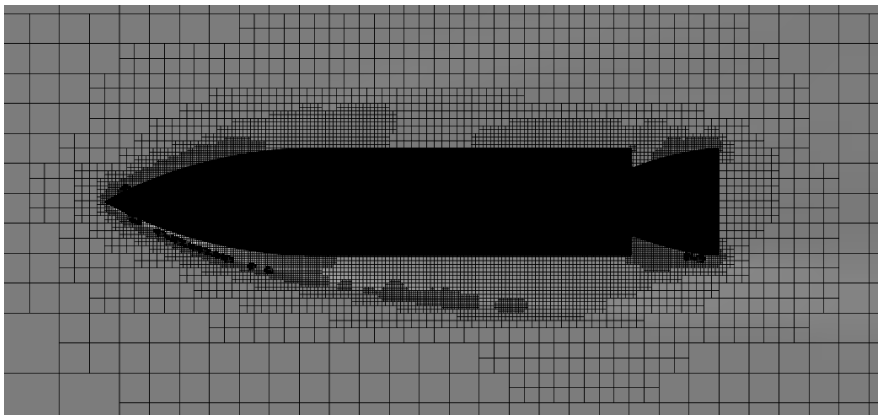

Figure 9. Adaptive mesh generated close to third stage rocket by CART3D for Mach 9, 10° angle of attack conditions.

$$\dot{\phi} = \frac{v \cos\gamma \sin\zeta}{r} \tag{5}$$

$$\dot{\gamma} = \frac{T \sin\alpha}{mv} + (\frac{v}{r} - \frac{\mu_E}{r^2 v}) \cos\gamma + \frac{L}{mv} + \cos\phi[2\omega_E \cos\zeta + \frac{\omega_E^2 r}{v}(\cos\phi\cos\gamma + \sin\phi\sin\gamma\sin\zeta)] \tag{6}$$

$$\dot{v} = \frac{T\cos\alpha}{mv} - \frac{\mu_E}{r^2}\sin\gamma - \frac{D}{m} + \omega_E^2 r \cos\phi(\cos\phi\sin\gamma - \sin\phi\cos\gamma\sin\zeta) \tag{7}$$

$$\dot{\zeta} = -\frac{v}{r}\tan\phi\cos\gamma\cos\zeta + 2\omega_E\cos\phi\tan\gamma\sin\zeta - \frac{\omega_E^2 r}{v\cos\gamma}\sin\phi\cos\phi\cos\zeta - 2\omega_E\sin\phi \tag{8}$$

III. Trajectory Optimisation

The three stages of the launch vehicle are simulated separately. This improves computational efficiency by allowing the optimisation to be considered as three problems that are coupled by the stage separation points:

- Determine the optimal trajectory of the first stage rocket from launch to first-second stage separation point ($\mathbf{x}_{1\to2}$)
- Determine the optimal trajectory of the second stage scramjet vehicle from $\mathbf{x}_{1\to2}$ to the second-third stage separation point ($\mathbf{x}_{2\to3}$)
- Determine the optimal trajectory for the third stage given $\mathbf{x}_{2\to3}$

Together these problems have the form of a sequential decision making problem, where the optimal solution can be determined using dynamic programming.[30] For this specific problem, the application of dynamic programming involves first optimising the first stage to determine the optimal separation point $\mathbf{x}_{1\to2}$ that gives maximum separation velocity at a set dynamic pressure. This is then treated as an initial constraint on the second stage optimisation, setting the initial altitude, velocity and Mach no of the second stage. The third stage is then simulated over a range of feasible separation conditions $\mathbf{x}_{2\to3}$ to create a list of corresponding payloads to orbit. A value function is computed efficiently by interpolating between separation conditions $\mathbf{x}_{2\to3}$, then this value function is treated as a terminal cost $C_3(\mathbf{x}_{2\to3})$ on the second stage trajectory.

III.A. First and Second Stage Optimisation

The optimal trajectory of the first and second stages has been determined separately. In both cases this has been achieved in both cases by selecting a control history $\mathbf{u}$:

$$\min_{\mathbf{u}} \quad C(\mathbf{x}, \mathbf{u}) + C_{a\to b}(\mathbf{x}_{a\to b}), \tag{9}$$

where $C(\mathbf{x}, \mathbf{u})$ is a continuous cost function and $\mathbf{C}_{a\to b}$ is a stage transition cost function dependent on the state variables $\mathbf{x}$ at the end of the trajectory. The optimisation of Equation 9 subject to the vehicle dynamics has the form of a Bolza optimisation problem, where an objective function $J(\mathbf{x}, \mathbf{u}, \tau_f)$ is minimised,

$$J(\mathbf{x}(\tau), \mathbf{u}(\tau), \tau_f) = \underbrace{M[\mathbf{x}(\tau_f), \tau_f]}_{C_{a\to b}(\mathbf{x}_{a\to b})} + \underbrace{\int_{\tau_0}^{\tau_f} P[\mathbf{x}(\tau), \mathbf{u}(\tau)]\, d\tau}_{C(\mathbf{x},\mathbf{u})}, \tag{10}$$

subject to a set of state dynamics $\dot{\mathbf{x}}(\tau)$, which describe the behaviour of the system over the solution space:

$$\dot{\mathbf{x}}(\tau) = f[\mathbf{x}(\tau), \mathbf{u}(\tau)] \tag{11}$$

and constrained by the boundary conditions $\boldsymbol{\psi}$ of the system at the initial and final time points:

$$\boldsymbol{\psi}_0[\mathbf{x}(\tau_0), \tau_0] = \mathbf{0}, \tag{12}$$

$$\boldsymbol{\psi}_f[\mathbf{x}(\tau_f), \tau_f] = \mathbf{0}. \tag{13}$$

The dynamics are also subject to a set of inequality constraints defining the bounds of the problem:

$$\boldsymbol{\lambda}[\mathbf{u}(t_k)] \leq \mathbf{0} \tag{14}$$

These bounds are chosen to span the possible operating ranges of the first stage and the SPARTAN to ensure an optimal solution. Solving this Bolza problem in a discrete simulation requires the use of numerical solution methods for which the pseudospectral method solver DIDO has been chosen.[31]

III.B. The Pseudospectral Method

The first and second stage trajectory solutions utilise the pseudospectral method, a form of direct spectral collocation.[17] The pseudospectral method offers good convergence properties and relatively good computational speed while not compromising the accuracy of the optimal solution.[32] These properties make the pseudospectral method appropriate for optimising a hypersonic vehicle system. The pseudospectral method utilises a spectral method approximation to convert the optimal control problem to be solved to partial differential equation form. The use of the spectral method ensures that higher order terms of the dynamic equations are solved, and allows solution with high accuracy, even with relatively few collocation points.[33] This method has been shown to be applicable to a variety of aerospace applications.[12,13,34,35]

III.C. Third Stage Optimisation

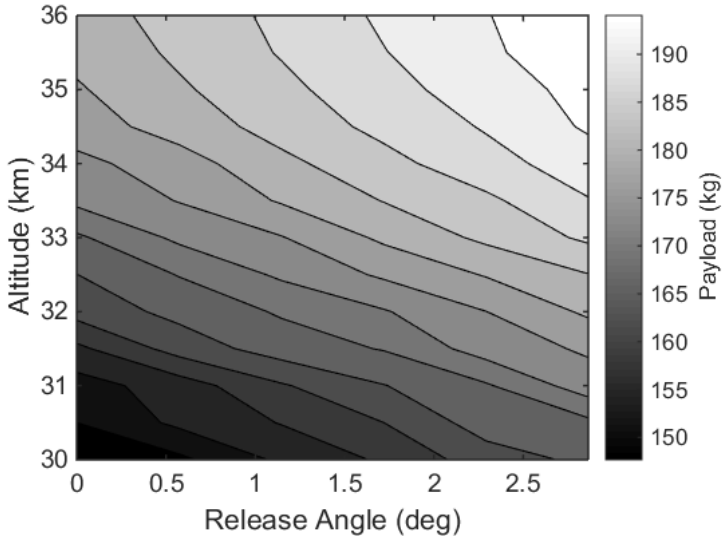

Figure 10. Payload mass results with variation in rocket stage release point for v = 2750m/s, heading angle = 1.70 rad and latitude = -0.1271 rad.

In order to increase the computational efficiency of the optimisation, it was decided to consider the third stage rocket as an end point cost of the scramjet stage trajectory, as opposed to optimising the entirety of the trajectory at once. Payload to orbit (used as the end cost for second stage optimisation, $C_3(\mathbf{x}_{2\rightarrow 3})$) was calculated over a 5 degree grid of separation conditions (velocity, altitude, trajectory angle, heading angle and latitude). For each condition, the in-atmosphere portion of the rocket stage trajectory is optimised for maximum payload to orbit using a 5 degree of freedom trajectory simulation. A simple minimum search is performed for three variables; burn time (t_b), angle of attack at start of burn ($\alpha_{3,2\rightarrow 3}$), and angle of attack at end of burn ($\alpha_{3,b}$). The MATLAB function fminsearch adjusts the values of these variables iteratively until an optimal payload to orbit is found. Payload to orbit results for a 2750m/s third stage release are shown in Figure 10.

IV. Results and Discussion

The program LODESTAR (Launch Optimisation and Data Evaluation for Scramjet Trajectory Analysis Research) has been developed to produce an optimal trajectory path for a rocket-scramjet-rocket launch vehicle. LODESTAR utilises DIDO[31] to optimise a trajectory towards a customisable objective (i.e. constant dynamic pressures or optimal payload mass). LODESTAR was used to investigate the suitability of a pseudospectral method approach to optimisation of scramjet-rocket trajectories. The following simulations were developed:

1. : q = 50kPa fixed SPARTAN trajectory
   → Verifies approach by comparison to previous results.

2. : Trajectory optimised for payload-to-orbit, q_{max} = 50kPa
   → Demonstrates the advantages of trajectory generation through coupled optimisation.

3. : Trajectory optimised for payload-to-orbit, q_{max} = 45kPa & q_{max} = 55kPa
   → Comparison of these simulations allows investigation into the effect of q max on payload-to-orbit.

4. : Trajectory optimised for payload-to-orbit, q_{max} = 50kpa, 110% SPARTAN Drag
   → Comparison of optimal trajectories at 100% and 110% drag allows investigation of the robustness of the solution with variation in vehicle design.

Table 1 details key results for comparison.

Table 1. Summary of Simulation Results

	1	**2**	**3a**	**3b**	**4**
Trajectory Condition	q = **50kPa**	$q \leq$ **50kPa**	$q \leq$ **45kPa**	$q \leq$ **55kPa**	$q \leq$ **50kPa, 110%** c_d
Payload to Orbit (kg)	166.7	198.6	193.8	200.3	190.1
Separation Alt 1→2 (km)	24.5	24.5	25.1	23.9	24.5
Separation v **1→2(m/s)**	1524	1524	1521	1524	1524
Separation Alt 2→3(km)	32.1	35.8	36.4	34.8	34.7
Separation v **2→3(m/s)**	2766	2759	2732	2780	2721
Separation γ **(deg)**	0.39	2.86	2.86	2.86	2.86
Separation q **(kPa)**	50.0	27.8	24.8	32.7	31.8
Separation L/d	3.02	3.29	3.38	3.24	2.99
2nd **Stage Flight Time (s)**	241.9	246.6	265.2	227.6	244.2
3rd **Stage Max** q **(kPa)**	52.3	27.8	24.8	32.7	31.8
3rd **Stage** $t >$ **20kpa (s)**	35.1	14.4	11.1	18.6	18.0

IV.A. First Stage Evaluation

Figure 11 shows the First stage optimised trajectory. The first stage rocket flies a fixed vertical trajectory for 20s, after which a pitchover is initiated. After pitchover the first stage is optimised using the pseudospectral method for maximum velocity at a specific separation dynamic pressure, with fuel limited to 15024kg. This

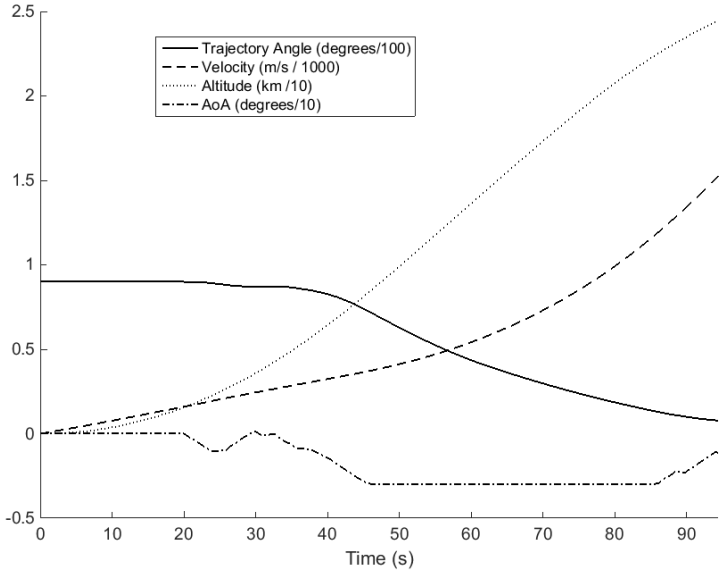

Figure 11. First stage trajectory, optimised for maximum velocity and a release point of 50kPa.

is achieved by setting a cost function that uses velocity directly, as well as a quadratic cost function centred around the desired dynamic pressure:

$$\min_{\mathbf{u}_2} \quad C_1(\mathbf{x}_{1\to 2}) \tag{15}$$

where

$$C_1(\mathbf{x}_{1\to 2}) = -v_{1\to 2} + (q_{1\to 2} - q_{desired})^2. \tag{16}$$

The angle of attack is limited to $\pm 3^\circ$ to produce a conservative estimate of vehicle capabilities. 50kPa dynamic pressure conditions are reached at 24.5km altitude and 1524m/s, after a total flight time of 94.4s. After pitchover a small adjustment is made between 20s and 29.9s, after which the angle of attack is reduced to -3°, and sustained until 85.4s, when the angle of attack is brought to zero and coast phase is initiated. Similar results were obtained for second stage release at 45kPa and 55kPa, with release points detailed in Table 1.

IV.B. Verification of LODESTAR - Fixed Dynamic Pressure Trajectory

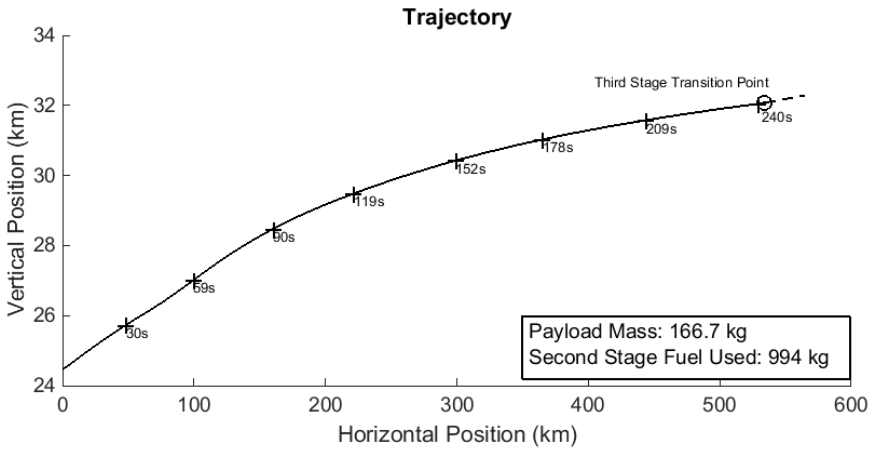

Figure 12. Trajectory path of the 2^{nd} stage SPARTAN vehicle flying at 50kPa constant dynamic pressure.

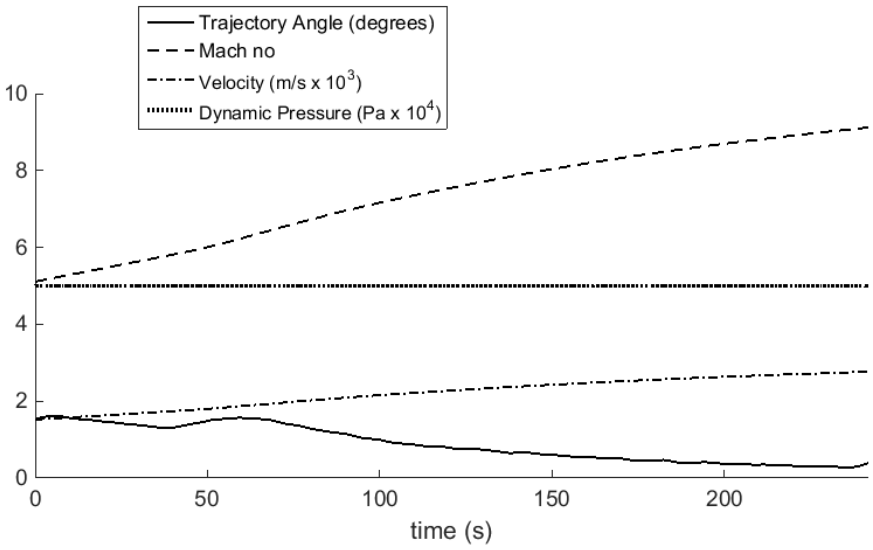

Figure 13. Trajectory data for 50kPa constant dynamic pressure trajectory.

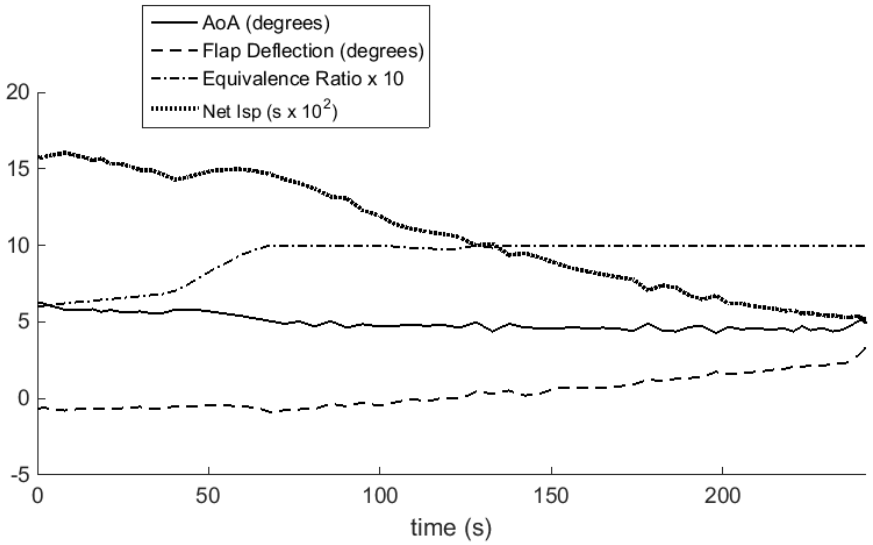

Figure 14. Vehicle performance data for 50kPa constant dynamic pressure trajectory. Note: Flap deflection is positive down.

A constant dynamic pressure trajectory was produced for verification of LODESTAR and to compare to existing results. This verification ensures that the vehicle model is consistent with existing simulations and that the optimiser is simulating the vehicle dynamics accurately. The trajectory was configured with a quadratic cost function centred around 50kPa dynamic pressure:

$$\min_{\mathbf{u}_2} \quad C_2(\mathbf{x}_2, \mathbf{u}_2) \tag{17}$$

$$C_2(\mathbf{x}_2, \mathbf{u}_2) = \int_{t_0}^{t_f} \frac{(\boldsymbol{q} - 50 \times 10^3)^2 + 50^4}{50^4} dt \tag{18}$$

The resulting constant dynamic pressure trajectory for the SPARTAN stage is shown in Figures 12, 13 and 14 with key results summarised in Table 1.

These results show very close adherence to 50kPa dynamic pressure (maximum 0.12% deviation) and close agreement with previous simulations of the SPARTAN vehicle controlled to q =50kPa using a Proportional-Integral-Derivative (PID) feedback controller.[36] The mean error in vertical trajectory position between

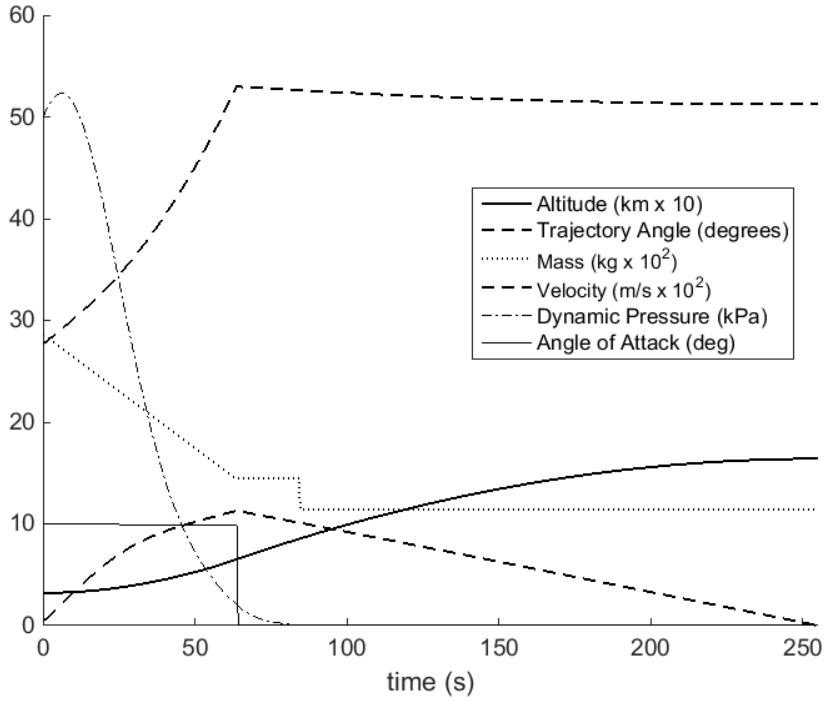

Figure 15. Third stage rocket trajectory simulated from the end of the 50kPa constant dynamic pressure SPARTAN trajectory.

LODESTAR and PID control[36] was found to be 0.48%, with a mean error in angle of attack of 0.41%. This close agreement indicates that LODESTAR is able to accurately simulate the scramjet vehicle throughout the trajectory.

Flying a constant dynamic pressure requires a low trajectory angle. This results in a third stage release angle of 0.39° to the horizontal. Over the 241.9s trajectory the Mach no. increases from 5.11 to 9.12 and the velocity from 1524m/s to 2766m/s. The flap deflection shows an overall increase from −1.0° to 2.7° over the trajectory, trimming the vehicle. The net specific impulse ($I_{sp_{net}} = \frac{T-F_d}{\dot{m}_f g}$) generally decreases over the trajectory, as the efficiency of the scramjet engines decreases. However, between 40.2s and 55.4s the net specific impulse increases, due to equivalence ratio increasing as the capture limitations are relaxed with increasing Mach number.

Figure 15 shows the corresponding third stage atmospheric exit trajectory after release at 50kPa, evaluated as described in Section II.C. After atmospheric exit, this trajectory is followed by a Hohmann transfer to a heliosynchronous orbit, resulting in a total payload to orbit of 166.7kg.

IV.C. Dynamic Pressure Limited Trajectory

LODESTAR was configured to optimise the total payload mass to orbit, by setting the cost functions accordingly:

$$\min_{\mathbf{u}_2} \quad C_2(\mathbf{x}_2, \mathbf{u}_2) + C_3(\mathbf{x}_{2\to 3}) \tag{19}$$

where

$$C_2(\mathbf{x}_2, \mathbf{u}_2) = 0.01 \int_{t_0}^{t_f} \dot{m}_f dt \tag{20}$$

$$C_3(\mathbf{x}_{2\to 3}) = -m_{payload} \tag{21}$$

In this case $C_3(\mathbf{x}_{2\to 3})$ is the trajectory target and is determined via interpolation of the third stage release point grid. $C_2(\mathbf{x}_2, \mathbf{u}_2)$ is included to improve numerical stability and has been chosen to have negligible effect on the resultant trajectory.

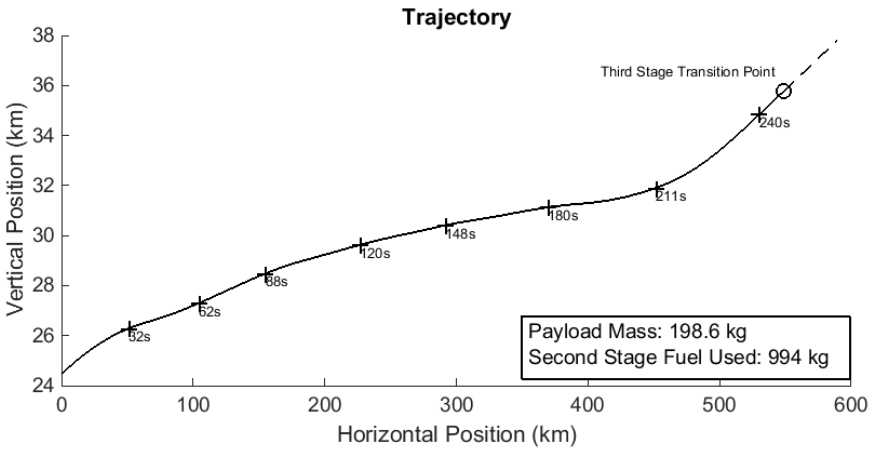

Figure 16. Maximum payload trajectory path of the 2^{nd} stage SPARTAN vehicle when limited to 50kPa dynamic pressure.

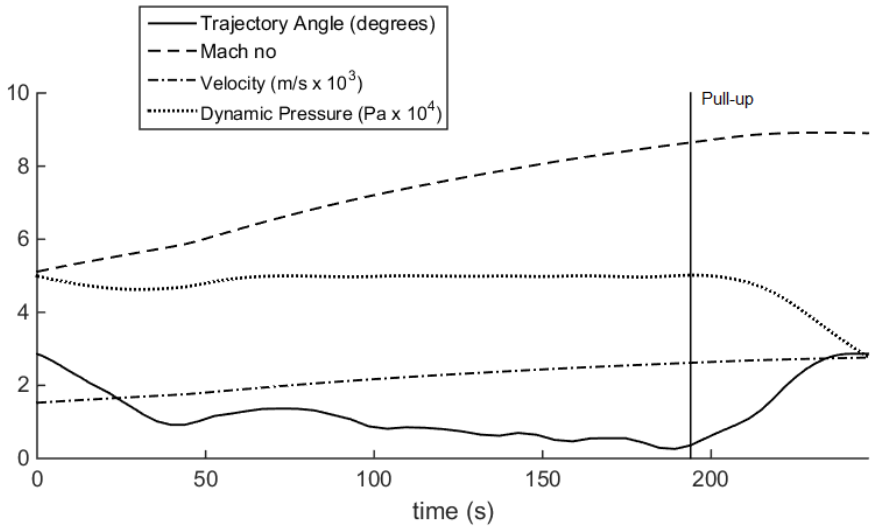

Figure 17. Trajectory data for 50kpa dynamic pressure limited trajectory.

A maximum dynamic pressure limit of 50kPa was applied to the optimisation process to allow direct comparison with the constant q trajectory and so that an equivalent vehicle can be used. This trajectory was limited to 0.05 radians (2.86°) maximum trajectory angle to capture a conservative estimate of vehicle capabilities, ie. a trajectory that is within the accepted operating region of the SPARTAN.

The optimal trajectory shape for a q =50kPa limited, maximum payload to orbit trajectory is shown in Figures 16, 17 and 18 with key results summarised in Table 1. The equivalence ratio of the engine is less than 1 until 52.6s, causing the SPARTAN to fly under 50kPa in this region (to a minimum of 48.8kPa) in order to maximise net specific impulse. After the equivalence ratio increases to 1, the trajectory follows a constant dynamic pressure path at 50kPa until 193.9s at which point a pull-up manoeuvre is performed, gaining altitude until rocket stage release at 246.6s flight time. This trajectory is able to deliver 198.6kg of payload to heliocentric orbit, an increase of 19.1% over the constant dynamic pressure result. The point at which the pull-up manoeuvre begins is the optimisation result that takes into account the best combination of velocity, altitude and release angle for scramjet stage performance and the release of the rocket stage. The constant rate of climb at the end of trajectory indicates the region at which increasing altitude and release angle becomes more important than extracting maximum thrust from the scramjet (which is attained at high q and low flight angle at an equivalence ratio of 1). Flight in a lower dynamic pressure environment results in less thrust output from the scramjet engines, as well as an increase in angle of attack and flap deflection angle to compensate for the additional lift required. Due to this, less overall acceleration is obtained compared

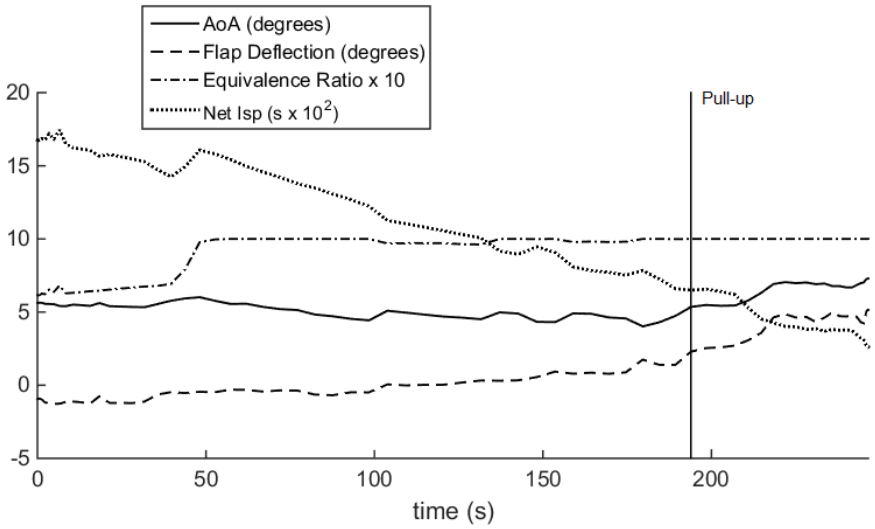

Figure 18. Vehicle performance data for 50kpa dynamic pressure limited trajectory. Note: Flap deflection is positive down.

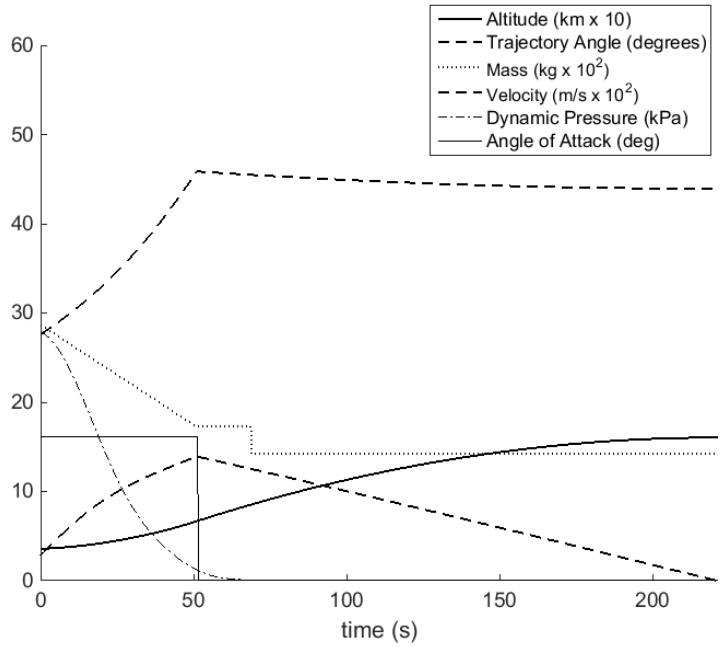

Figure 19. Third stage rocket trajectory simulated from the end of the 50kPa dynamic pressure limited maximum payload SPARTAN trajectory.

to the constant dynamic pressure result. Separation occurs at a velocity of 2759m/s, a decrease of 7m/s. However, separation altitude increases by 3.7km to 35.8km, resulting in a decreased separation dynamic pressure of 27.8kPa.

The scramjet stage pull-up assists the rocket in manoeuvring to exoatmospheric altitude by increasing the altitude and angle at separation by virtue of the increased L/d ratio and manoeuvrability of the scramjet vehicle. Even a small increase in release angle to 2.86° significantly reduces the turning that is required by the rocket as evident from comparing Fig 15 and 19, lessening the time that the rocket must spend in a high dynamic pressure environment, and decreasing the maximum dynamic pressure that the rocket stage experiences by 44.4%, as shown in Table 1. The benefit of increasing trajectory angle at the release point on the payload mass to orbit is clearly shown in Figure 10. Similarly, decreasing dynamic pressure at release decreases the structural mass and heat shielding necessary to achieve exoatmospheric flight.

Compared to studies considering vehicles with a scramjet-rocket transition within a single stage[9],[10] the maximum payload to orbit trajectory of the multi-stage system shows a scramjet-rocket transition point at much lower altitudes. This lower transition point is a consequence of the stage separation creating an energy trade-off which does not occur in a single stage vehicle. In the multi-stage system, the optimal separation point is dependent on utilising the superior aerodynamic performance and engine efficiency of the scramjet stage, while trading-off the energy cost of increasing the altitude of the scramjet stage. Past a certain point, the energy required to increase the altitude of the scramjet stage is not offset by the performance benefits, and staging occurs. This beneficial ability to separate the scramjet stage results in a lower scramjet-rocket transition point when compared to single stage vehicle designs. Single stage vehicles must necessarily transport all components to exoatmosphere, and so utilise the scramjet engines until higher altitude to take advantage of their high efficiency.

IV.D. Dynamic Pressure Sensitivity

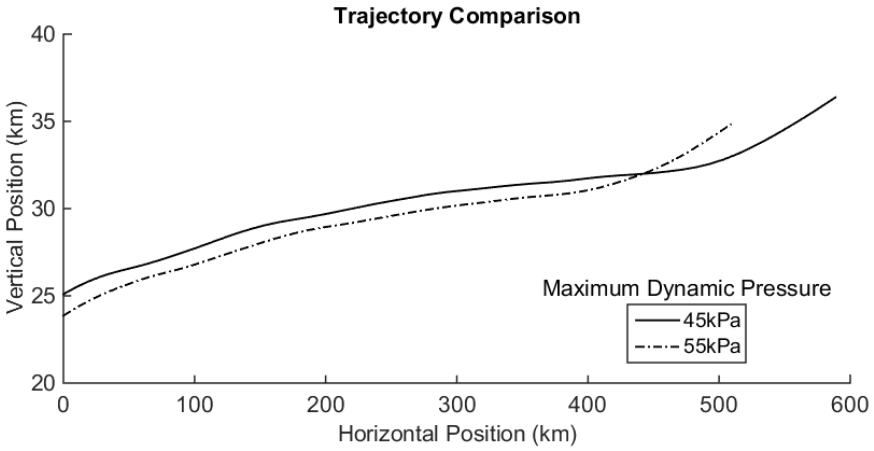

Figure 20. Comparison of 45kPa / 55kpa dynamic pressure limited trajectory paths for maximum payload to orbit.

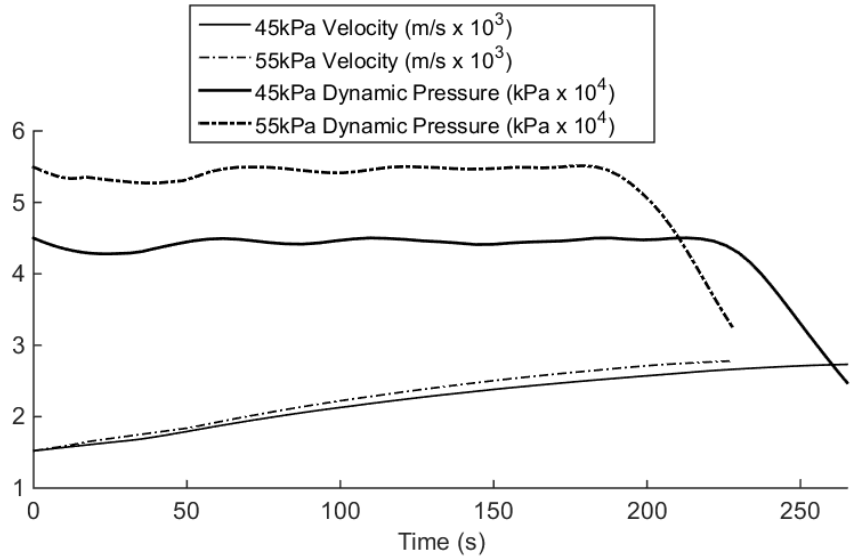

Figure 21. Comparison of trajectory data for 45kPa / 55kpa dynamic pressure limited trajectories.

To investigate the sensitivity of the vehicle to changes in q_{max}, the maximum dynamic pressure was varied to 45kPa and 55kPa and the flight trajectory optimised, with results shown in Figures 20, 21 and 22 and summarised in Table 1. The ±10% variation in maximum dynamic pressure has been shown to have

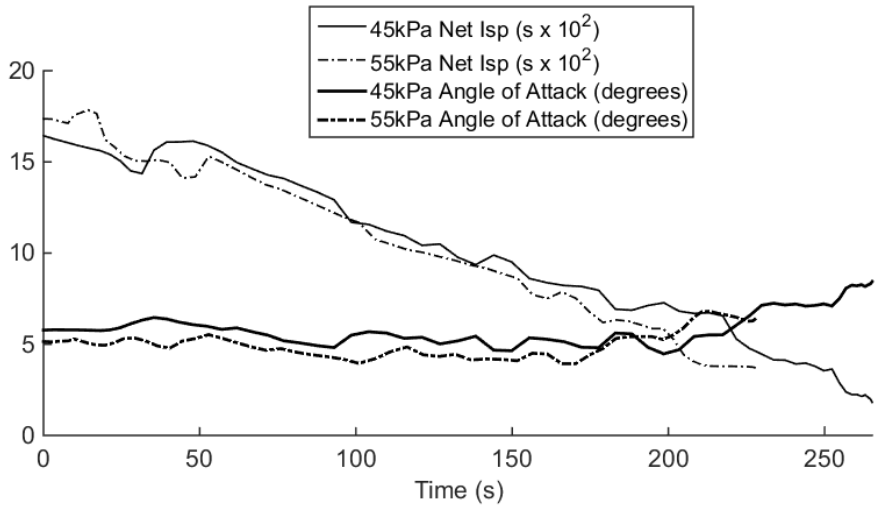

Figure 22. Comparison of vehicle performance data for 45kPa / 55kpa dynamic pressure limited trajectories.

very little effect on the payload mass delivered to heliocentric orbit. Varying the maximum dynamic pressure by ±5kPa from 50kPa causes a variation of only +1.7 kg(+0.86%) or −4.8 kg(−2.42%) in payload to orbit.

Both trajectories use 994kg of fuel, and reach separation altitudes of 36.4km and 34.8km with separation velocities of 2732m/s and 2780m/s for 45kPa and 55kPa respectively. Flying at a lower dynamic pressure limit allows a pull-up into higher altitude, with relatively small variation in separation velocity (+21m/s or −27m/s). This small variation in velocity is despite the increase in air density and decrease in angle of attack required for flight at 55kPa dynamic pressure, both of which increase the mass flow into the engine. Although the thrust output of the REST engines increases with dynamic pressure, so does the drag on the vehicle, and the net increase in performance is small.

Only small variation in optimal payload mass has been observed, without modification of vehicle design to account for dynamic pressure limit. This indicates that designing and operating a vehicle at lower dynamic pressures may be preferable. Flying at a lower maximum dynamic pressure allows reduction of the structural weight and heat shielding of the vehicle. Additionally, flying at low dynamic pressure allows the third stage to be released into lower dynamic pressure, lessening the structural and heat shielding requirements on the third stage rocket.

IV.E. Lift/Drag Ratio Sensitivity Analysis

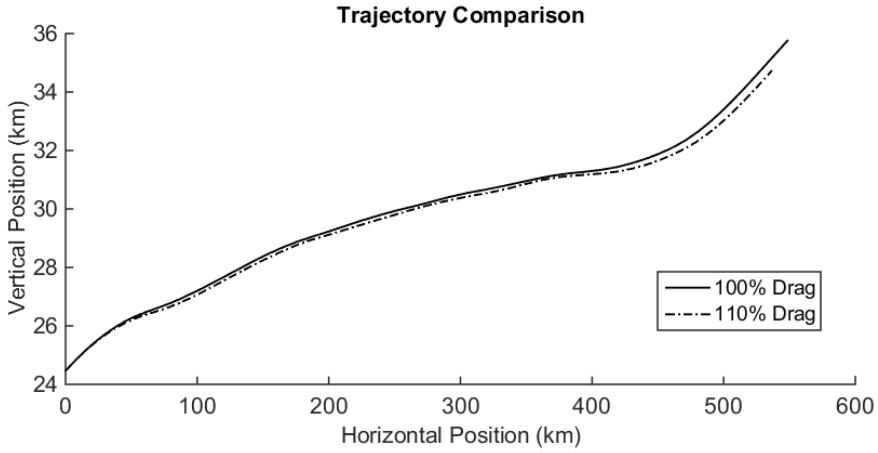

Figure 23. Comparison of trajectory paths for 100% and 110% drag cases for a 50kPa dynamic pressure limited maximum payload trajectory.

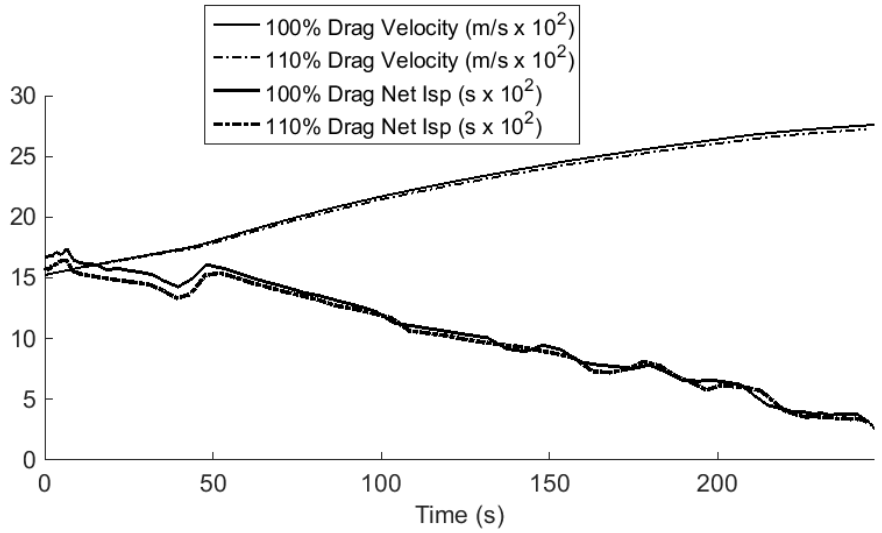

Figure 24. Comparison of v and $I_{sp_{net}}$ for 100% and 110% drag cases for a 50kPa dynamic pressure limited maximum payload trajectory.

To investigate the effect of vehicle design and uncertainty in aerodynamic performance on the optimal trajectory the drag on the vehicle was increased by 10%, and an optimised trajectory calculated with dynamic pressure limited to 50kpa. Selected results are compared to the baseline result (dynamic pressure limited to 50kPa) in Figures 23 and 24. These results show that when drag is increased (ie. L/d is decreased) the high drag second stage lags behind the base-line trajectory and follows a slightly slower and hence lower flight path. The net result is a lower payload-to-orbit of 190.1kg (a decrease of 4.3%). Though the separation point varies, the shape of the pull-up manoeuvre that occurs for the increased drag case is very similar to that of the baseline case. This similarity suggests that a pull-up manoeuvre is optimal for multiple vehicle designs. Additionally, the similar payload-to-orbit results indicate that re-optimisation of the trajectory is an effective way to mitigate the effects of significant changes in vehicle design or uncertainties in vehicle aerodynamics, although so far only the effect of second stage vehicle drag on payload to orbit has been investigated. The results have shown that the net impact of increased scramjet stage drag on the payload to orbit is rather small, particularly if one considers that the highest drag losses occur during the second stage flight.

V. Conclusions

In this paper an optimal control program, LODESTAR, has been used to optimise the trajectory of a rocket-scramjet-rocket multi-stage system. This system consists of a rocket powered first stage, modelled on a scaled down Falcon-1; the SPARTAN, a scramjet accelerator being developed at the University of Queensland; and a rocket powered third stage. For the simulated system, LODESTAR has been validated against traditional feedback control. Applied to full trajectory optimisation LODESTAR has been able to generate optimised trajectory simulations that increase performance of the multi-stage system.

Results indicate that a pull-up manoeuvre at the end of a constant dynamic pressure trajectory is the optimal scramjet flight path for a system transitioning between separate airbreathing and rocket-powered stages. The optimal pull-up manoeuvre trades off velocity (a decrease of 7m/s) for altitude (an increase of 3.7km), and was found to increase payload mass to heliocentric orbit by 31.9kg (19.1%). The pull up manoeuvre was also found to limit third stage dynamic pressure to 27.8kPa, a decrease of 44.4% compared to a trajectory with no pull-up. This decrease in maximum dynamic pressure decreases the stress experienced by the rocket stage proportionally, as well as decreasing the heat flux into the rocket, both of which lead to significant benefits for the design of the rocket stage. A decrease in structural stress allows for less internal reinforcement, and a decrease in heat flux allows for reduction of the heat shield size, resulting in further increases in payload mass.

As part of a dynamic pressure sensitivity evaluation, the maximum dynamic pressure limit of the vehicle was varied by ±5kPa. This was found to produce only a +0.86% and −2.42%variation on the payload

mass delivered to orbit. This small variation in payload-to-orbit indicates that a scramjet powered stage designed for operation at lower dynamic pressure may be advantageous. If efficient, low dynamic pressure scramjet engines are available, operating at lower dynamic pressure enables lighter vehicles due to reduced structural and thermal loads. This reduction in mass potentially leads to further performance improvements and operational benefits including increased payload to orbit and extended range.

To investigate the effect of changes in second stage vehicle properties, the drag of the scramjet was increased by 10% and the optimal trajectory evaluated. It was found that a pull-up manoeuvre occurred with a lower second-third stage transition point when compared to the original result, indicating that the rocket is favoured at an earlier point in the climb manoeuvre. This variation in the optimal trajectory was minor, indicating that the trajectory shape presented is robust with respect to changes in vehicle design and, by extension, changes in engine performance or vehicle aerodynamics. Thus re-optimisation of the trajectory while taking account of the new aerodynamic performance is a good approach to minimise impacts on the aggregate performance of the system.

Overall this work has provided new insight into the preferred operating ranges for scramjet vehicles incorporated in multi-stage to orbit systems.

Acknowledgments

The authors would like to thank Dawid Preller for his work on the SPARTAN vehicle which was integral to this study.

References

[1]Office of Commercial Space Transportation (AST) and the Commercial Space Transportation Advisory Committee (COMSTAC), *2001 Commercial Space Transportation Forecasts*, No. May, Office of Commercial Space Transportation, Washington, DC, 2001.

[2]Smart, M. K. and Tetlow, M. R., "Orbital Delivery of Small Payloads Using Hypersonic Airbreathing Propulsion," *Journal of Spacecraft and Rockets*, Vol. 46, No. 1, 2009, pp. 117–125.

[3]Heiser H. H. and Pratt, D. T., *Hypersonic Airbreathing Propulsion*, American Institute of Aeronautics and Astronautics, Washington, D.C, 1994.

[4]Flaherty, K. W., Andrews, K. M., and Liston, G. W., "Operability Benefits of Airbreathing Hypersonic Propulsion for Flexible Access to Space," *Journal of Spacecraft and Rockets*, Vol. 47, No. 2, 2010, pp. 280–287.

[5]Kimura, T. and Sawada, K., "Three-Stage Launch System with Scramjets," *Journal of Spacecraft and Rockets*, Vol. 36, No. 5, 1999, pp. 675–680.

[6]Olds, J. and Budianto, I., "Constant Dynamic Pressure Trajectory Simulation with POST," *Aerospace Sciences Meeting & Exhibit*, Reno, NV, 1998, pp. 1–13.

[7]Preller, D. and Smart, M. K., "Scramjets for Reusable Launch of Small Satellites," *20th AIAA International Space Planes and Hypersonic Systems and Technologies Conference*, No. July, Glasgow, Scotland, 2015, pp. 1–23.

[8]Powell, R. W., Shaughnessy, J. D., Cruz, C. I., and Naftel, J. C., "Ascent performance of an air-breathing horizontal-takeoff launch vehicle," Vol. 14, No. 4, 1991, pp. 834–839.

[9]Lu, P., "Inverse dynamics approach to trajectory optimization for an aerospace plane," *Journal of Guidance, Control, and Dynamics*, Vol. 16, No. 4, 1993, pp. 726–732.

[10]Trefny, C., "An Air-Breathing Concept Launch Vehicle for Single-Stage-to-Orbit," *35th Joing Propulsion Conference and Exhibit*, No. May, Los Angeles, CA, 1999.

[11]Mehta, U. B. and Bowles, J. V., "Two-Stage-to-Orbit Spaceplane Concept with Growth Potential," *Journal of Propulsion and Power*, Vol. 17, No. 6, 2001, pp. 1149–1161.

[12]Bedrossian, N., Technologies, B., and Nasa, L. N., "Zero Propellant Maneuvre Flight Results For 180 Degree ISS Rotation," *20th International Symposium on Space Flight Dynamics*, Annapolis, MD, 2007.

[13]Josselyn, S. and Ross, I. M., "Rapid Verification Method for the Trajectory Optimization of Reentry Vehicles," *Journal of Guidance, Control, and Dynamics*, Vol. 26, No. 3, 2002, pp. 505–508.

[14]Sekhavat, P., Fleming, A., and Ross, I., "Time-optimal nonlinear feedback control for the NPSAT1 spacecraft," *Proceedings, 2005 IEEE/ASME International Conference on Advanced Intelligent Mechatronics.*, Monterey, CA, 2005, pp. 24–28.

[15]Ranieri, C. L. and Ocampo, C. a., "Optimization of Roundtrip, Time-Constrained, Finite Burn Trajectories via an Indirect Method," *Journal of Guidance, Control, and Dynamics*, Vol. 28, No. 2, 2005, pp. 306–314.

[16]Elnagar, G., Kazemi, M. a., and Razzaghi, M., "The Pseudospectral Legendre Method for Discetizing Optimal Control Problems," *IEEE Transactions on Automatic Control*, Vol. 40, No. 10, 1995, pp. 1793–1796.

[17]Fahroo, F. and Ross, I., "Direct trajectory optimization by a Chebyshev pseudospectral method," *Proceedings of the 2000 American Control Conference.*, Vol. 6, Chicago, IL, 2000, pp. 3860–3864.

[18]Aftosmis, M. J., Berger, M. J. and Adomavicius, G., "A Parallel Multilevel Method for Adaptively Refined Cartesian Grids with Embedded Boundaries," *38th Aerospace Sciences Meeting and Exhibit*, Reno NV, 2000.

[19]Aftosmis, M. J. and Berger, M. J., "Robust and efficient Cartesian mesh generation for component-based geometry Robust and Efficient Cartesian Mesh Generation for Component-Based Geometry," *Aerospace*, , No. January, 1997.

[20]Mehta, U., Aftosmis, M., Bowles, J., and Pandya, S., "Skylon Aerodynamics and SABRE Plumes," *20th AIAA International Space Planes and Hypersonic Systems and Technologies Conference*, , No. July, 2015, pp. 1–21.

[21]Aftosmis, M. J., Nemec, M., and Cliff, S. E., "Adjoint-based low-boom design with Cart3D," *29th AIAA Applied Aerodynamics Conference 2011*, , No. June, 2011, pp. 1–17.

[22]PTC, "www.ptc.com," 2017.
[23]Pointwise, "www.pointwise.com," 2017.
[24]Jazra, T., Preller, D., and Smart, M. K., "Design of an Airbreathing Second Stage for a Rocket-Scramjet-Rocket Launch Vehicle," *Journal of Spacecraft and Rockets*, Vol. 50, No. 2, 2013, pp. 411–422.
[25]Jazra, T. and Smart, M., "Development of an Aerodynamics Code for the Optimisation of Hypersonic Vehicles," *47th AIAA Aerospace Sciences Meeting Including The New Horizons Forum and Aerospace Exposition*, Orlando, Florida, 2009, p. 2009.
[26]NASA, *U.S. Standard Atmosphere, 1976*, U.S. Government Printing Office, Washington, D.C., 1976.
[27]Suraweera, M. and Smart, M. K., "Shock Tunnel Experiments with a Mach 12 {REST} Scramjet at Off-Design Conditions," *Journal of Propulsion and Power*, Vol. 25, No. 3, 2009, pp. 555–564.
[28]Gollan, R. J. and Smart, M. K., "Design of Modular , Shape-transitioning Inlets for a Conical Hypersonic Vehicle," *Aerospace, AIAA*, Vol. 29, No. 4, 2013, pp. 832–838.
[29]Pontani, M. and Teofilatto, P., "Simple Method for Performance Evaluation," *Acta Astronautica*, Vol. 94, No. 1, 2014, pp. 434–445.
[30]Bertsekas, D. P., *Dynamic Programming and Optimal Control, Volume I*, Athena Scientific, Belmont, MA, 2005.
[31]Ross, I. M., *A Beginners Guide to DIDO (ver 7.3): A MATLAB Application Package for Solving Optimal Control Problems*, Elissar, LLC, Monterey, CA.
[32]Fasano, G. and Pinter, J., *Modelling and Optimisation in Space Engineering*, Springer, New York, NY, 2013.
[33]Fahroo F. & Ross, I., "Computational Optimal Control By Spectral Collocation With Differential Inclusion .." *1999 Flight Mechanics Symposium*, , No. May, 1999, pp. 185–200.
[34]Huntington, G. T. and Rao, A. V., "Optimal Reconfiguration of Spacecraft Formations Using the Gauss Pseudospectral Method," *Journal of Guidance, Control, and Dynamics*, Vol. 31, No. 3, 2008, pp. 689–698.
[35]Yan, H., Ross, I. M., and Alfriend, K. T., "Pseudospectral Feedback Control for Three-Axis Magnetic Attitude Stabilization in Elliptic Orbits," *Journal of Guidance, Control, and Dynamics*, Vol. 30, No. 4, 2007, pp. 1107–1115.
[36]Preller, D. and Smart, M. K., "Longitudinal Control Strategy for Hypersonic Accelerating Vehicles," *Journal of Spacecraft and Rockets*, Vol. 52, No. 3, 2015, pp. 1–6.